

A TRAINED NETWORK SOLUTION FOR MULTI- STATE STRUCTURAL AWARENESS

Michael Todd and Zhu Mao

**The Regents of the University of California
University of California, San Diego
9500 Gilman Drive, Mail Code 0934
La Jolla, CA 92093-0934**

12 March 2012

Final Report

APPROVED FOR PUBLIC RELEASE; DISTRIBUTION IS UNLIMITED



**AIR FORCE RESEARCH LABORATORY
Space Vehicles Directorate
3550 Aberdeen Ave SE
AIR FORCE MATERIEL COMMAND
KIRTLAND AIR FORCE BASE, NM 87117-5776**

DTIC COPY NOTICE AND SIGNATURE PAGE

Using Government drawings, specifications, or other data included in this document for any purpose other than Government procurement does not in any way obligate the U.S. Government. The fact that the Government formulated or supplied the drawings, specifications, or other data does not license the holder or any other person or corporation; or convey any rights or permission to manufacture, use, or sell any patented invention that may relate to them.

This report is the result of contracted fundamental research deemed exempt from public affairs security and policy review in accordance with SAF/AQR memorandum dated 10 Dec 08 and AFRL/CA policy clarification memorandum dated 16 Jan 09. This report is available to the general public, including foreign nationals. Copies may be obtained from the Defense Technical Information Center (DTIC) (<http://www.dtic.mil>).

AFRL-RV-PS-TR-2011-0172 HAS BEEN REVIEWED AND IS APPROVED FOR
PUBLICATION IN ACCORDANCE WITH ASSIGNED DISTRIBUTION STATEMENT

//signed//
WHITNEY REYNOLDS
Program Manager

//signed//
BRETT J. DEBLONK, Ph.D.
Technical Advisor, Spacecraft Component Technology Branch

//signed//
B. SINGARAJU, Ph.D.
Deputy Chief, Spacecraft Technology Division
Space Vehicles Directorate

This report is published in the interest of scientific and technical information exchange, and its publication does not constitute the Government's approval or disapproval of its ideas or findings.

Approved for public release; distribution is unlimited.

| REPORT DOCUMENTATION PAGE | | | | Form Approved OMB No. 0704-0188 | |
|---|-----------------------------|--------------------------------|----------------------------|---|---|
| Public reporting burden for this collection of information is estimated to average 1 hour per response, including the time for reviewing instructions, searching existing data sources, gathering and maintaining the data needed, and completing and reviewing this collection of information. Send comments regarding this burden estimate or any other aspect of this collection of information, including suggestions for reducing this burden to Department of Defense, Washington Headquarters Services, Directorate for Information Operations and Reports (0704-0188), 1215 Jefferson Davis Highway, Suite 1204, Arlington, VA 22202-4302. Respondents should be aware that notwithstanding any other provision of law, no person shall be subject to any penalty for failing to comply with a collection of information if it does not display a currently valid OMB control number. PLEASE DO NOT RETURN YOUR FORM TO THE ABOVE ADDRESS. | | | | | |
| 1. REPORT DATE (DD-MM-YY) 09-03-2012 | | 2. REPORT TYPE Final Report | | 3. DATES COVERED (From - To) 15 Jan 2009 – 29 Dec 2011 | |
| 4. TITLE AND SUBTITLE A Trained Network Solution for Multi-State Structural Awareness | | | | 5a. CONTRACT NUMBER FA9453-09-1-0315 | |
| | | | | 5b. GRANT NUMBER | |
| | | | | 5c. PROGRAM ELEMENT NUMBER MIPR | |
| 6. AUTHOR(S) Michael Todd and Zhu Mao | | | | 5d. PROJECT NUMBER MIPR | |
| | | | | 5e. TASK NUMBER PPM00005112 | |
| | | | | 5f. WORK UNIT NUMBER EF003018 | |
| 7. PERFORMING ORGANIZATION NAME(S) AND ADDRESS(ES) The Regents of the University of California University of California, San Diego 9500 Gilman Drive, Mail Code 0934 La Jolla, CA 92093-0934 | | | | 8. PERFORMING ORGANIZATION REPORT NUMBER | |
| 9. SPONSORING / MONITORING AGENCY NAME(S) AND ADDRESS(ES) Air Force Research Laboratory Space Vehicles Directorate 3550 Aberdeen Ave., SE Kirtland AFB, NM 87117-5776 | | | | 10. SPONSOR/MONITOR'S ACRONYM(S) AFRL/RVSV | |
| | | | | 11. SPONSOR/MONITOR'S REPORT NUMBER(S) AFRL-RV-PS-TR-2011-0172 | |
| 12. DISTRIBUTION / AVAILABILITY STATEMENT Approved for public release; distribution is unlimited. | | | | | |
| 13. SUPPLEMENTARY NOTES | | | | | |
| 14. ABSTRACT This project considered a rapid condition assessment test using transmissibility measurements in vibration tests. A hypothesis test is established that detects changes in transmissibility estimations over time that indicate target failure mode occurrence; in this project, fastener preload loss was the first considered failure mode for simple representations of satellite structures, and later consideration was given to cracking in beam-like rotor structures. Inherent to this procedure (or any structural health monitoring application) is the quantification of uncertainty in order to obtain maximal probability of detection while minimizing the probability of false alarms. Within the specific applications just cited, a set of novel statistical models were developed which resulted in actual probability density function derivations for transmissibility measurements (considering both estimation error and extraneous environmental noise-induced error). These probability density functions could then be used to establish quantitative thresholds that helped establish rigorous probability-of-detection-based hypothesis testing that suggest optimal testing procedures for detecting damage when using transmissibility as a feature. | | | | | |
| 15. SUBJECT TERMS structural health monitoring, vibration testing, transmissibility, uncertainty quantification, statistical modeling | | | | | |
| 16. SECURITY CLASSIFICATION OF: | | | 17. LIMITATION OF ABSTRACT | 18. NUMBER OF PAGES | 19a. NAME OF RESPONSIBLE PERSON |
| a. REPORT Unclassified | b. ABSTRACT Unclassified | c. THIS PAGE Unclassified | | | Whitney Reynolds |
| | | | Unlimited | 32 | 19b. TELEPHONE NUMBER (include area code) |

(This page intentionally left blank)

TABLE OF CONTENTS

| Section | Page |
|--|------|
| List of Figures..... | ii |
| 1.0 SUMMARY..... | 1 |
| 2.0 INTRODUCTION..... | 2 |
| 3.0 TESTING OF TRANSMISSIBILITY AS A FEATURE SOURCE..... | 4 |
| 4.0 STATISTICAL UNCERTAINTY MODELING APPROACHES..... | 6 |
| 4.1 Perturbation Approach..... | 7 |
| 4.2 Gaussian Bivariate Approach..... | 8 |
| 4.3 Chi-square Bivariate Approach..... | 10 |
| 5.0 RECEIVER OPERATING CHARACTERISTICS..... | 13 |
| 6.0 PHASE UNCERTAINTY MODEL..... | 16 |
| 7.0 CONCLUSIONS..... | 22 |
| 8.0 RECOMMENDATIONS AND FUTURE WORK..... | 22 |
| REFERENCES..... | 24 |

LIST OF FIGURES

| Figure | Page |
|--------|--|
| 1 | Finite element model (left) and first mode of structure (right).....4 |
| 2 | Fastened and unfastened area (left) and damaged mode shape (right).....5 |
| 3 | Metric evaluations for 1% spring stiffness loss.....6 |
| 4 | General SIMO data flow.....7 |
| 5 | Transmissibility estimation in noise-excitation test.....8 |
| 6 | Metrics for detecting change in transmissibility.....8 |
| 7 | Three degree-of-freedom system for validation.....9 |
| 8 | Single-channel transfer function magnitudes with estimation and uncertainty bounds...10 |
| 9 | Transmissibility estimation between mass #1 and #2 (left) and outlier percentage (right).....10 |
| 10 | Beam model for statistical model validation.....11 |
| 11 | Histogram of transmissibility estimation and derived probability density function.....12 |
| 12 | Transmissibility estimation with predicted 90% confidence boundaries; 1% NSR.....12 |
| 13 | Probability density function of transmissibility estimations for different damage levels: 0.87 Hz, 0% NSR (upper left); 0.87 Hz, 1% NSR (mid left); 0.87 Hz 10% NSR (lower left); 3.12 Hz, 0% NSR (upper right); 3.12 Hz, 1% NSR (mid right); 3.12 Hz 10% NSR (lower right).....14 |
| 14 | ROC curves for different frequencies and settings with $n_d=4$: 0.87 Hz, 0% NSR (upper left); 0.87 Hz, 1% NSR (mid left); 0.87 Hz 10% NSR (lower left); 3.12 Hz, 0% NSR (upper right); 3.12 Hz, 1% NSR (mid right); 3.12 Hz 10% NSR (lower right).....15 |
| 15 | AUC metric evaluation vs. frequency: 0% NSR (left), 1% NSR (middle), 10% NSR (right).....15 |
| 16 | Comparison of AUC for different damage levels and NSRs.....16 |
| 17 | Plate structure.....17 |
| 18 | Magnitude of transfer function H at each measurement point.....18 |
| 19 | Phase of transfer function H at each measurement point.....18 |
| 20 | Transmissibility T for 1-2 and 3-4.....19 |
| 21 | Histogram of phase estimation for H and T at arbitrary frequency lines.....19 |
| 22 | Magnitude of transfer function H at each measurement point.....20 |
| 23 | Metrics of transfer function phase estimation.....21 |
| 24 | Metrics of transmissibility phase estimation.....21 |

1.0 SUMMARY

This project considered building risk-informed decision-making with regard to vibration tests used for any sort of qualification procedure, maintenance action, or state assessment. Using a single-input/multi-output state model with output noise on each channel, three separate statistical models were derived for the estimation of the transmissibility function, both with extraneous noise (such as from the environment, measurement system, etc.) and without extraneous noise (only considering the error in the estimation procedure itself). The three models were based on different applications of transmissibility estimators, including a perturbation approach, a Gaussian bivariate approach, and a Chi-square bivariate approach.

This project commenced in January 2009 with a simple finite element model simulation that showed the capability of transmissibility estimation from rapid vibration testing in the application of damage detection and structural health monitoring (specifically for detecting fastener preload loss and stiffness changes). Two features were proposed, namely root mean square error and dot product difference. Because of the nature of transmissibility, it is more sensitive for local changes and therefore transmissibility-based features are better at capturing small damages.

The three statistical models mentioned above were then derived and compared. The model via perturbation approach simply supplies the variance and bias error for one of the transmissibility estimators, which requires the least information about input and output. Gaussian bivariate approach gives a more accurate quantification through cross power density estimations, except in very small frequency range, where the magnitude is really low and does not deliver lots of useful information. Chi-square bivariate approach delivers the most accurate statistical model and does not require any information from the input, but when extraneous noise level is high, the estimator itself is submerged under noise floor, and does not contain useful transmissibility information. Furthermore, although this approach had overall the best features, it only works for transmissibility magnitude estimations. All comparisons were validated on a three-degree-of-freedom system model.

Based upon the statistical models established, a receiver operating characteristic (ROC) analysis was applied to evaluate performance, and the conclusion was reached that at frequency lines with good input-output gain, the detection is globally stable even when there is noise contamination.

Phase estimation statistical modeling work commenced for both frequency response function and transmissibility. Similar validation has been done with data from a cantilevered plate structure. Test results show clearly the sensitivity of transmissibility phase in capturing structural parameter changes, although this study was still ongoing at the time of funding loss.

2.0 INTRODUCTION

The initial thrust was determined to be investigation of possible rapid testing/check-out procedures that could be implemented for satellite verification readiness (responsive to significantly reduced time required for qualification). Funding sources later changed to Army Research Laboratory (ARL), which had a shift in focus to risk-informed detection of damage for maintenance and operations purposes in rotorcraft. Common to both applications is some form of state assessment or system identification [1], often in the frequency domain [2]. For mechanical/structural system identification processes, approaches in the frequency domain require vibration-based testing (e.g., experimental modal analysis via the FRF) to obtain the relationship between structural parameters (mass, stiffness, and damping), the characteristic eigenstate (resonant frequencies, mode shapes, and sometimes damping), and measured vibration response [3]. Any frequency domain approach that relies on FRF estimation, however, requires either direct measurement of or an assumption of the input excitations to the system. It is well-known that for some applications such measurements are impossible or difficult to obtain, and/or such assumptions would be poor or inappropriate; for these situations, estimation of a transmissibility function is possible. Similar to a traditional input-output transfer function such as the FRF, the transmissibility function is defined as the frequency-domain ratio between two outputs, and it describes the relative admittance between the two measurements. Devriendt et al. interpret the transmissibility concept versus transfer function as response data normalized by a reference response instead of by the input excitation [4]. The transmissibility also contains less general but more specific (local) information compared to the FRF, because the characteristic polynomial, which contains all the system poles (resonances), will be cancelled in calculating transmissibilities, and only the system zeros (anti-resonances) will remain. Therefore, transmissibility-derived features are entirely independent of system poles but solely dependent on zeros. Unlike the system resonances, which are influenced by structural parameters globally, system anti-resonances are more affected by local properties and are more sensitive to detailed structural modeling and change detection (such as for damage identification). As a result, transmissibility appears to be a useful characteristic in identification with more sensitivity to local structural details and effects [5, 6].

A generalization of the transmissibility concept was introduced by Ribeiro et al. [7]. For a multi-DOF structure, the transmissibility can be derived from the FRF matrix, where the FRF matrix is obtained from either testing or analytical/numerical modeling. This relates the set of measureable coordinates and the set of interest coordinates together and makes the identification process more convenient. Mottershead [8] suggested a useful alternative for modal analysis and demonstrated that the sensitivity of the zeros estimated from response measurements and FRF estimations may be expressed as linear combinations of the sensitivities of natural frequencies and mode shapes, where the closer modes contribute more to the sum. He et al. [9] studied the sensitivity about

local mass and stiffness with respect to the anti-resonance locations when applying relocation of zeros for vibration reduction purposes.

One application area receiving lots of attention is using transmissibility estimation for better quality modal parameter evaluation. Considering the operational modal analysis context with output-only measurements available, Devriendt et al. [6] successfully generalized the modal identification process where the excitation can be any type of input, not constrained to be a white noise sequence; by combining transmissibility data under different loading conditions, they show a good consistency between the modal parameters estimated from transmissibility measurements and the actual system poles. They report that by considering two different transmissibility estimations corresponding to the same positions but with different input excitation, the estimations cross each other at the system resonances, which means different estimations are exactly the same value at system poles. This value is directly related to scalar mode shapes and is used for modal parameter extraction in a multiple-input/multiple-output (MIMO) procedure and for accurate system poles localization [4, 10].

Transmissibility-based system identification, for many of the reasons described above, is also getting increased attention in the area of damage detection and structural health monitoring [11-13]. Johnson et al. apply transmissibility-based diagnostic technology to reduce the dimension of response measurements and demonstrate analytically and experimentally the sensitivity of transmissibility to both linear and nonlinear system changes [5, 11], as well as significantly enhanced localization capability since the system zeros are only sensitive to the parameters in certain localized region, and anti-resonance frequencies show significant variations with different measurement positions [5, 14]. Worden et al. [13, 15] implement system damage/fault detection via neural network training and outlier analysis, demonstrating that the system transmissibility provides a sensitive feature for the detection of small stiffness variation. Therefore, with the transmissibility-based technique, it is straightforward to identify the appearance and location of the system parameter changes. System identification results have shown that the localization is effective on both discrete [5] and continuous [14] system applications. Worden et al. [16-18] go through the entire process of experimental validation of a structural health monitoring methodology, based upon the measured transmissibilities and novelty detection. The investigation expands from simple laboratory structures to complex and realistic structures such as aircraft wing, and both the results from detection and localization are validated.

For all practical applications, of course, inherent to any such assessment is the quantification of uncertainty, as it is well known the sensitivity of any feature derived from transmissibility (or any other system identification quantity such as the FRF) is compromised by noise, generally categorized into four classes: operational, environmental, measurement, and computational [19]; these compromised estimates may lead to significant false-positive (Type-I) errors in the interpretation of system identification results, regardless of specific application. In this paper, the

primary objective is, under an assumed single-input/multiple-output (SIMO) vibration test and estimator, to propose a statistical model for uncertainty bounds and to derive the actual distribution of estimates of the transmissibility function. Most of the previous works involved with uncertainty quantification in system identification procedures are focused on the modeling of the FRF and input-output transfer function uncertainty. With a Gaussian input and optimized channel assumption, Bendat and Piersol's classic works derived the standard deviation of different estimations with respect to the coherence function, through which the uncertainty bounds for different confidence levels could be expressed approximately in a Gaussian way [20-22]. In Ref. [23], an extended model with uncorrelated noise is introduced, which is applicable to evaluate the uncertainty of complex FRFs. Under appropriate hypotheses, Goodman [24, 25] formulated the confidence bands for all elements in the FRF matrix approximately using an F -distribution, and the confidence bands are also given as functions of coherence.

However, the transmissibility function, which is the ratio of two correlated output power spectra, is not generally accurately modeled with Gaussian or F -distribution characteristics. This project considers a particular transmissibility estimator and derives an exact probability density function for uncertainties associated with its computation, including the influence of corrupting external noise sources. In fact, three different models for different transmissibility estimators are derived, and they are compared and evaluated for performance. The best selection is further validated experimentally, and global performance stability is assessed via a receiver operating characteristic (ROC).

3.0 TESTING OF TRANSMISSIBILITY FEATURE SOURCE

Motivated by the advantages of transmissibility as a sensitive quantity representing structure status, a simplified satellite model was first considered. A cubic shell (plate)-frame assembly was designed in ABAQUS, with the mesh plotted in Figure (1-left.) Preliminary analysis was deployed based upon modal analysis, in order to observe possible changes in dynamic behavior between completely fastened and unfastened states.

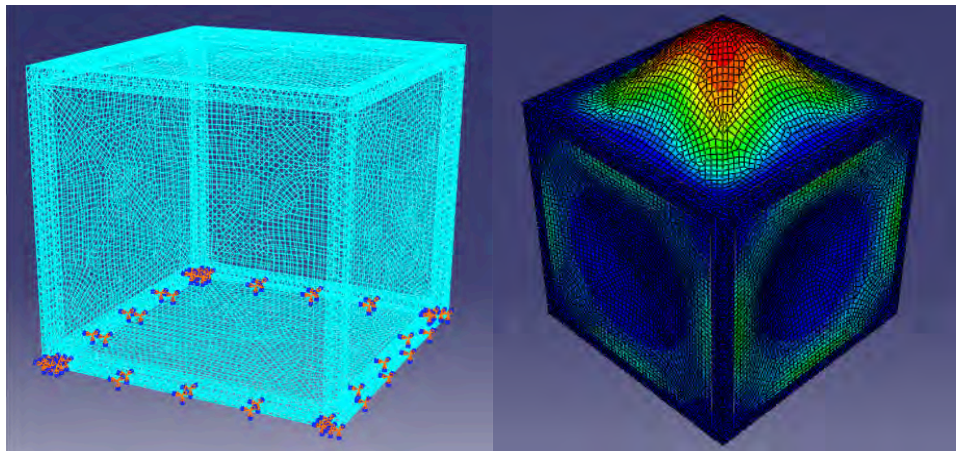


Figure 1: Finite element model (left), and first mode of the structure (right).

When a local region is unfastened, the initial hypothesis is that modal properties would change. Figure 2 shows such a (subtle) change for a particular mode shape, where there is a subtle loss in the shape symmetry, as well as local strain concentrations.

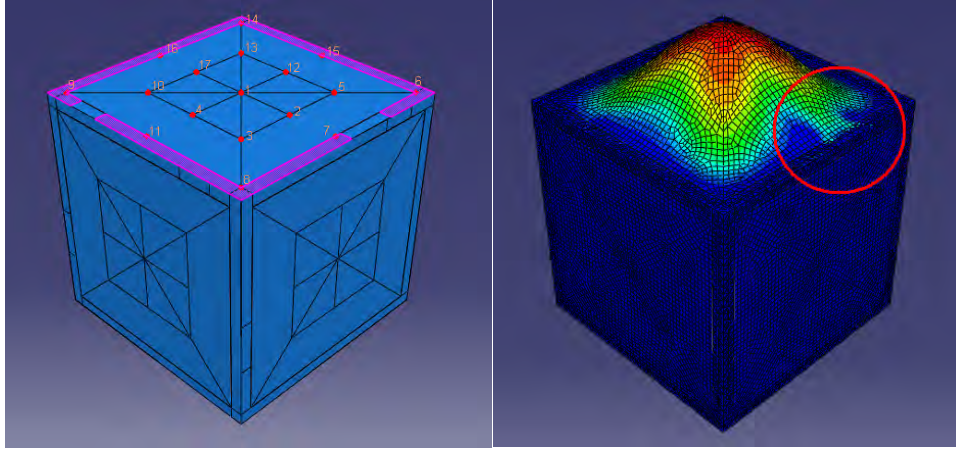


Figure 2: Fastened area in pink and local unfastened area (left), and damaged mode shape (right).

Motivated by the observed (localized) changes to the modal spatial structure as preload loss occurs, the transmissibility transfer function was chosen magnitude as a departure point for analysis. The transmissibility is described thus as the magnitude of the frequency domain transfer function $T_{ij}(\omega)$ between any two acceleration measurement points a_i and a_j , or

$$T_{ij}(\omega) = \left| \frac{FFT(a_i)}{FFT(a_j)} \right|. \quad (1)$$

Transmissibility essentially detects relative magnitude (and phase for certain estimators) changes that are occurring among any combination of measurement points. In order to quantify the change of transmissibility magnitude, more compactly, two evaluation metrics were considered. One is the root-mean-square error E_{ij} (RMSE), defined as:

$$E_{ij} = \sqrt{\frac{1}{n-1} \sum_n \left(\Delta T_{ij}(\omega_n) - \bar{\Delta T}_{ij} \right)^2}, \quad \Delta T_{ij} = T_{ij, \text{fastened}} - T_{ij, \text{unfastened}}. \quad (2)$$

And a second metric considers the projection of the fastened and unfastened transmissibilities via the dot product, normalized subsequently by the length of the feature vectors:

$$\cos \theta_{ij} = \frac{T_{ij, \text{fastened}}(\omega) \cdot T_{ij, \text{unfastened}}(\omega)}{\|T_{ij, \text{fastened}}(\omega)\| \|T_{ij, \text{unfastened}}(\omega)\|}. \quad (3)$$

For simplification, the final second metric was defined as $1 - |\cos \theta_{ij}|$. Compared to the RMSE metric, this metric has the advantage of scaling between 0 and 1.

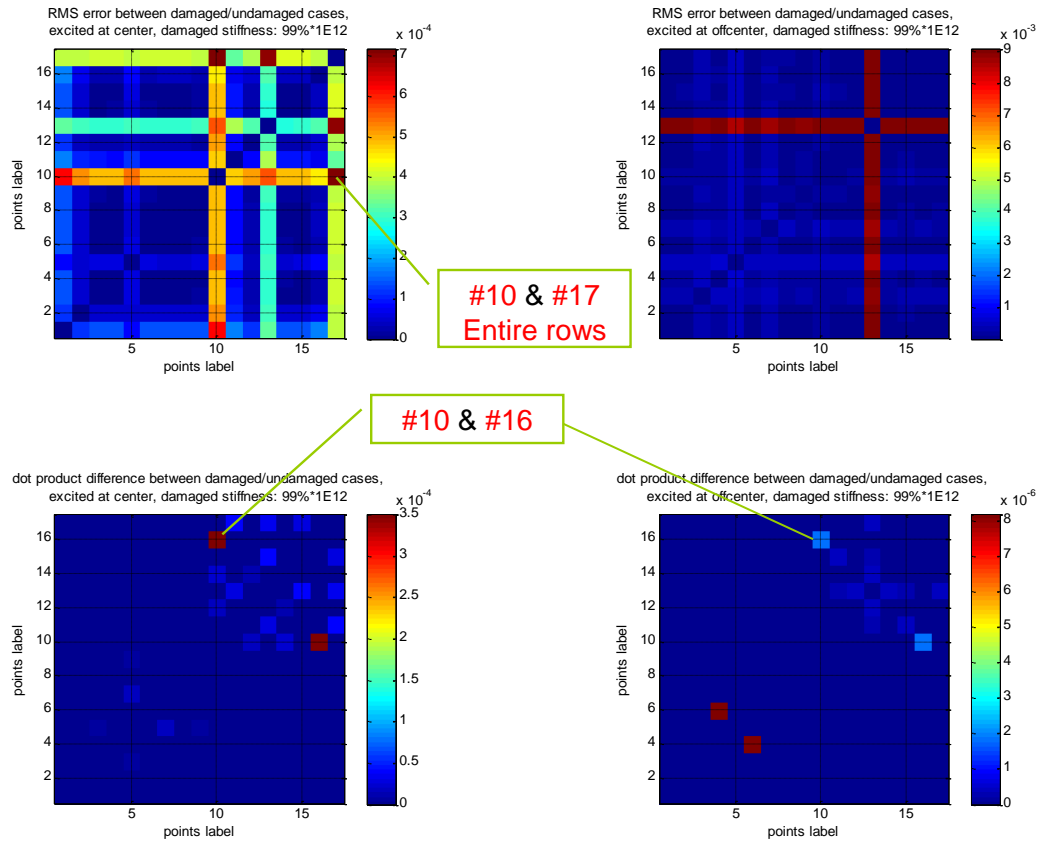


Figure 3: Metric evaluations for 1% spring stiffness loss.

Figure 3 is the two metric evaluations for 1% of spring stiffness loss (damage), with excitation at center/off center positions, about which preliminary conclusions were made in previous interim reports.

The two metrics are capable to detect structural parameter changes that indicate damage occurrence; however, when the system is subject to noise contamination or the transmissibility is estimated via shaker test with non-deterministic excitation, the transmissibility may undergo a non-damage-induced change. Under this circumstance, statistical uncertainty quantification is required in order to filter out the false alarms and produce a confidence level for decision-making.

4.0 STATISTICAL UNCERTAINTY MODELING APPROACHES

A single-input-multiple-output (SIMO) flow describes how transmissibility is derived and contaminated by extraneous noise, as shown in Figure 4, where the output in the context of this project is, but not limited to, acceleration.

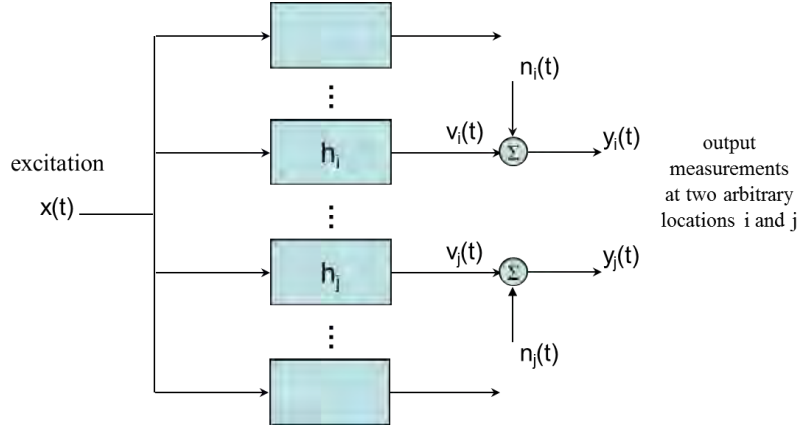


Figure 4: General SIMO data flow.

Three fundamental statistical approaches were derived and considered for modeling uncertainty:

4.1 Perturbation Approach

Using assumed small values of noise and Gaussian-distributed features, estimations on the variance and bias were derived

$$\text{Var} \left[\left| \hat{T}_{ij} \right| \right] \approx \frac{\left(1 - \sqrt{\gamma_{y_i y_j}^2} \right)}{\sqrt{\gamma_{y_i y_j}^2} \cdot n_d} \left| T_{ij} \right|^2, \text{ and } b \left[\left| \hat{T}_{ij} \right| \right] \approx \sqrt{\gamma_{y_i y_j}^2} - 1, \quad (4)$$

where $\gamma_{y_i y_j}^2$ is coherence between the two measurements and n_d is the number of averages. This model has a special assumption that $\gamma_{v_1 y_2}^2 = \gamma_{y_1 v_2}^2 = \sqrt{\gamma_{y_1 y_2}^2}$, which may not be accurate for all the conditions. However, for good signal-to-noise cases, this relation approximately holds, and this model was applied to the data from structural simulation of the previous ABAQUS model with Gaussian random noise added to the acceleration responses. Figure 5 shows an example of the transmissibility magnitude for structure in Figure 1, and the 1-sigma boundaries are plotted in green dots.

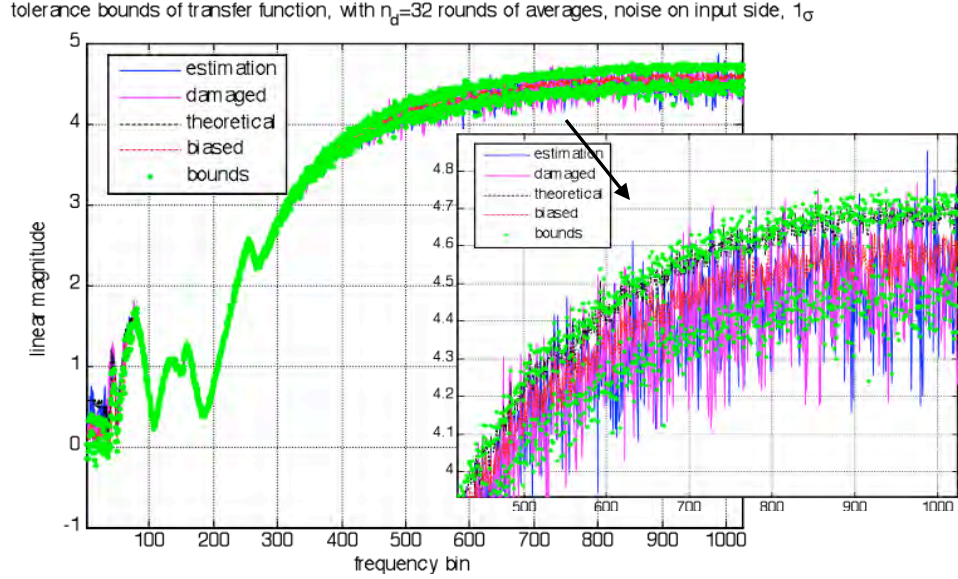


Figure 5: Transmissibility estimation in noise-excitation test.

Since the change in transmissibility for this case is difficult to observe visually in Figure 5, the average percentage of outliers and distance between outliers and corresponding boundaries (root-mean-square error) was used to quantitatively represent the transmissibility change. Figure 6 clearly classifies the two groups of measurements into damaged and undamaged conditions for both metrics. When there is no stiffness loss at all, the two groups of data fall perfectly on top of each other.

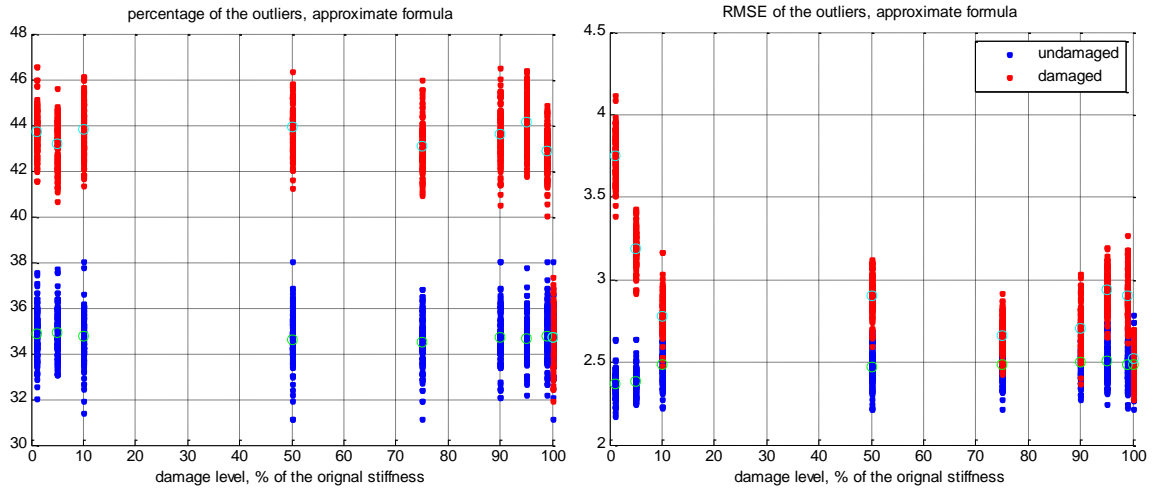


Figure 6: Metrics for detecting change of transmissibility.

4.2 Gaussian Bivariate Approach

Considering the transmissibility estimator $T_{ij} = H_i/H_j$, a Gaussian bivariate model was considered, in which transmissibility magnitude is regarded as ratio of two Gaussian random

variables. Denoting $\left| \hat{H}_i \right| : N(\mu_i, \sigma_i)$ and $\left| \hat{H}_j \right| : N(\mu_j, \sigma_j)$, and random variable $z = \left| \hat{H}_i \right| / \left| \hat{H}_j \right|$, the probability density function of z is given by:

$$f(z) = \frac{1}{\pi} \cdot \frac{\sigma_i \sigma_j \sqrt{1-r^2}}{\sigma_j^2 - 2rz\sigma_i\sigma_j + z^2\sigma_i^2} \cdot e^{-\frac{1}{2} \frac{1}{1-r^2} \left(\frac{\mu_i^2}{\sigma_i^2} - 2r \frac{\mu_i \mu_j}{\sigma_i \sigma_j} + \frac{\mu_j^2}{\sigma_j^2} \right)}$$

$$+ \frac{\sigma_j (r\mu_j\sigma_i - \mu_i\sigma_j) + z\sigma_i (r\mu_i\sigma_j - \mu_j\sigma_i)}{\pi \sqrt{(\sigma_j^2 - 2rz\sigma_i\sigma_j + z^2\sigma_i^2)^3}} \cdot e^{-\frac{1}{2} \frac{(\mu_j - z\mu_i)^2}{\sigma_j^2 - 2rz\sigma_i\sigma_j + z^2\sigma_i^2}} \cdot \int_0^{\frac{\sigma_j (r\mu_j\sigma_i - \mu_i\sigma_j) + z\sigma_i (r\mu_i\sigma_j - \mu_j\sigma_i)}{\sigma_i \sigma_j \sqrt{(1-r^2)(\sigma_j^2 - 2rz\sigma_i\sigma_j + z^2\sigma_i^2)}}} e^{-\frac{1}{2}u^2} du$$

...(5)

$$\text{where } \mu_i = E\left[\left| \hat{H}_i \right|\right] = \frac{G_{xv_i}}{G_{xx}} \text{ and } \mu_j = E\left[\left| \hat{H}_j \right|\right] = \frac{G_{xv_j}}{G_{xx}};$$

$$\sigma_i = \varepsilon\left[\left| \hat{H}_i \right|\right] \cdot \mu_i \text{ and } \sigma_j = \varepsilon\left[\left| \hat{H}_j \right|\right] \cdot \mu_j;$$

$$\varepsilon\left[\left| \hat{H}_i \right|\right] \approx \sqrt{\frac{1-\gamma_{xy_i}^2}{2 \cdot n_d \cdot \gamma_{xy_i}^2}} \text{ and } \varepsilon\left[\left| \hat{H}_j \right|\right] \approx \sqrt{\frac{1-\gamma_{xy_j}^2}{2 \cdot n_d \cdot \gamma_{xy_j}^2}}.$$

The statistical model in Equation (5) was validated through a simpler lumped parameter mass-spring-damper system, whose transfer function and transmissibility are analytically available for better validation/comparison.

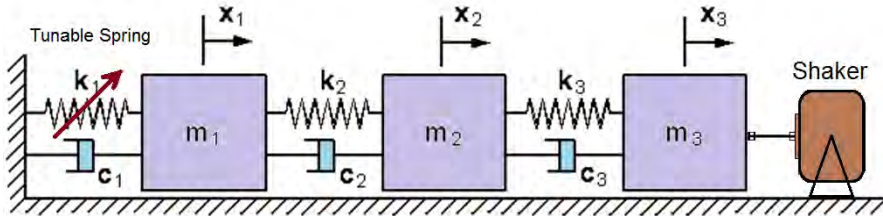


Figure 7: Three degree-of-freedom system for validation.

Figure 8 plots the input-output transfer function estimations, when the system in Figure 7 is excited at degree-of-freedom (DOF) #3, and outputs at DOF #1 and DOF #2, with the 1-standard deviation boundary plotted in red.

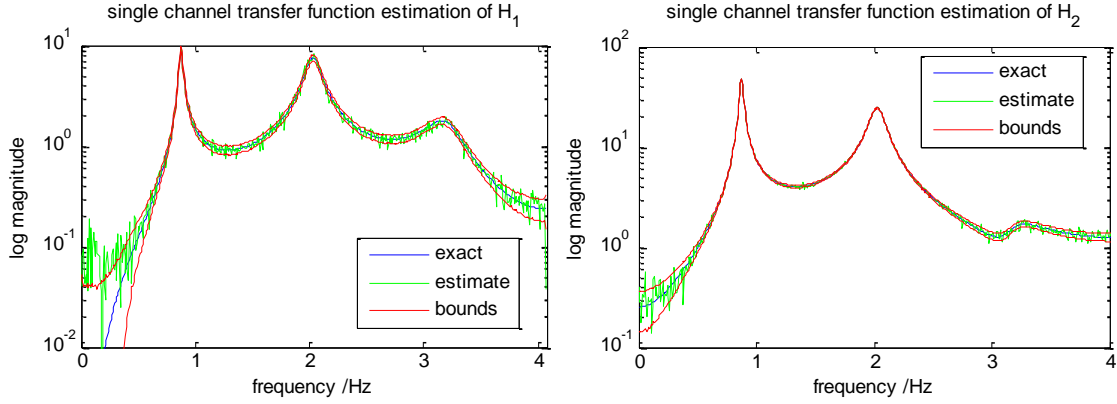


Figure 8: Single channel transfer function magnitudes with estimation and uncertainty bounds.

Figure 9 plots the transmissibility estimation and 90%-confidence bounds, which are given by Equation (5), and similar to the perturbation approach, the outlier percentage is calculated and plotted in Figure 9.

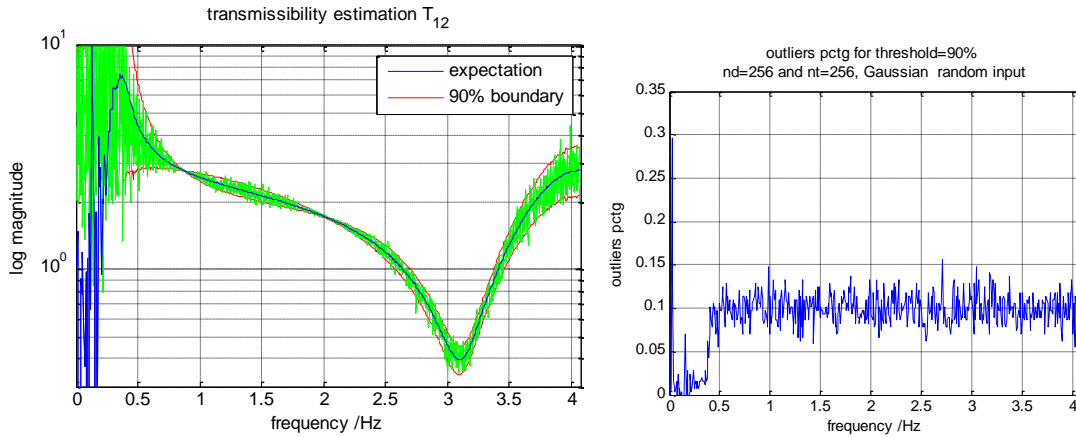


Figure 9: Transmissibility estimation between mass #1 and #2 (left) and outlier percentage (right).

Excellent consistency of outliers (10%) was observed, since the confidence interval of the uncertainty boundaries was set at 90%. The reason for the poor accuracy in the frequency range lower than 0.5Hz is because of the large skewness for the estimation distribution when the magnitude, always positive by definition, is very small. The probability model does allow for negative magnitude changes, and this physical inconsistency, while very small, does corrupt low-amplitude estimations.

4.3 Chi-square Bivariate Approach

This approach models the uncertainty in the most accurate way, where the estimator in Equation (6) is adopted and the transmissibility can be regarded as the square root of the ratio between two Chi-square random variables:

$$T_{ij} = \sqrt{\frac{G_{y_i y_i}}{G_{y_j y_j}}} = \sqrt{\frac{G_{v_i v_i} + G_{n_i n_i}}{G_{v_j v_j} + G_{n_j n_j}}}. \quad (6)$$

The probability density function of auto-power density and transmissibility are given by Equation (7) and (8) respectively:

$$p_{\chi^2}(z; 2n_d) = \frac{z^{n_d-1} \cdot e^{-\frac{z}{2}}}{2^{n_d} \cdot \Gamma(n_d)}; \quad (7)$$

$$p_t(\hat{T}) = \frac{2^{2n_d} \hat{T}^{(2n_d-1)} \left((1-\rho^2) \sigma_{Y_i}^2 \sigma_{Y_j}^2 \right)^{n_d} \Gamma\left(n_d + \frac{1}{2}\right)}{\sqrt{\pi} \left(\sigma_{Y_i}^2 + \hat{T}^2 \sigma_{Y_j}^2 \right)^{2n_d} \left(1 - \frac{4\hat{T}^2 \rho^2 \sigma_{Y_i}^2 \sigma_{Y_j}^2}{\left(\sigma_{Y_i}^2 + \hat{T}^2 \sigma_{Y_j}^2 \right)^2} \right)^{n_d + \frac{1}{2}} \Gamma(n_d)}, \quad (8)$$

where $\rho = \sqrt{\frac{C_{Y_i Y_j}^2 + C_{Y_i Y_j}^2}{\sigma_{Y_i}^2 \sigma_{Y_j}^2}}.$

Similar to the Gaussian approach, validation was performed on a continuous beam, whose analytical transfer function and transmissibility are also available, as shown in Figure 10. The statistical model in Equations (7) and (8) were both validated by various confidence thresholds and different noise contamination levels. Figure 11 shows observed histogram of transmissibility compared to the predicted probability density function at an arbitrary frequency line, with expectation (average), 5%, and 95% feature boundaries in green.

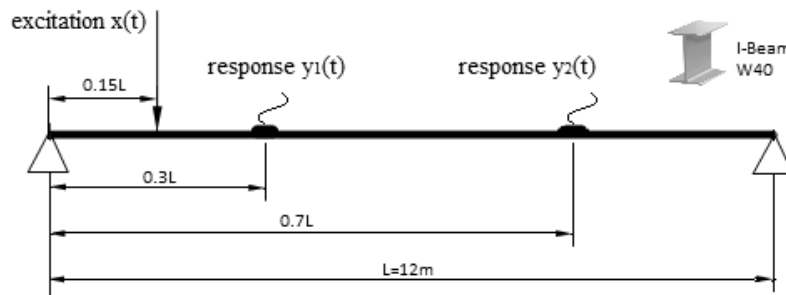


Figure 10: Beam model for statistical model validation.

Figure 12 shows an example of transmissibility estimation over the frequency domain and the predicted 90% confidence boundaries, with 1% of noise contamination. Outlier percentage over the entire frequency domain is also plotted in Figure 12, where an exact consistency is obtained between the histogram observation and the model prediction.

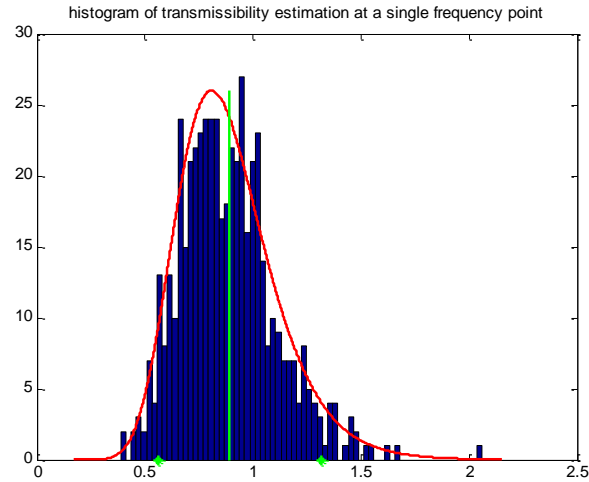


Figure 11: Histogram of transmissibility estimation and derived probability density function.

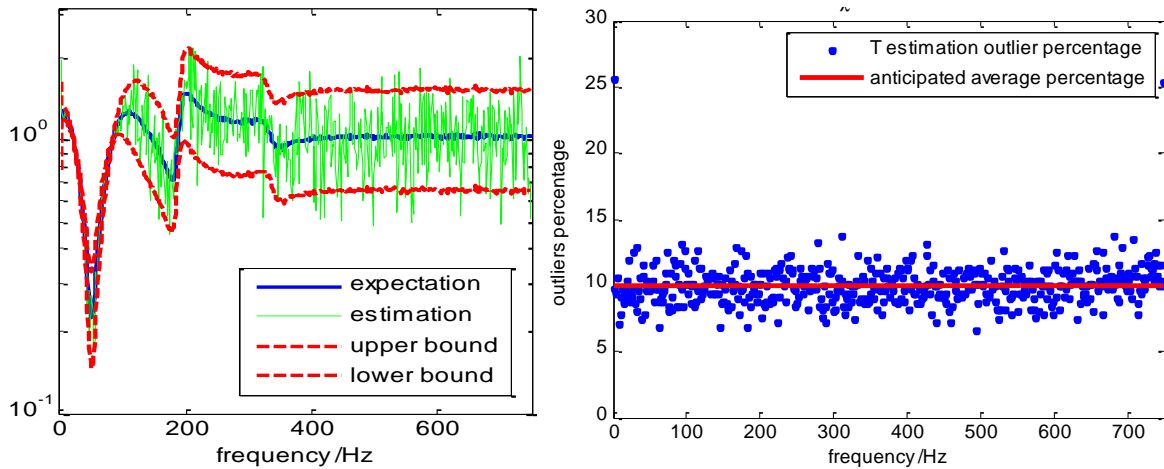


Figure 12: Transmissibility estimation with predicted 90% confidence boundaries, 1% of NSR.

Thus, three statistical models quantifying uncertainty of transmissibility magnitude estimation have been established, and Table 1 compares the pros and cons of each approach. Chi-square bivariate approach has the best accuracy and compatibility with output-only data, but is not as robust as other approaches for noise-contaminated conditions.

Table 1: Comparison between different quantification approaches.

| | Perturbation | Gaussian bivariate | Chi-square bivariate |
|---------------------------|---|---|---|
| estimator | $\sqrt{\hat{G}_{y_i y_i} / \hat{G}_{y_j y_j}}$ | \hat{H}_i / \hat{H}_j | $\sqrt{\hat{G}_{y_i y_i} / \hat{G}_{y_j y_j}}$ |
| assumption | Optimized channels Uncorrelated noise Balanced channels | Uncorrelated noise | No assumptions |
| input knowledge required? | no | yes | no |
| distribution form | Gaussian | Ratio of correlated Gaussian | Square root of the ratio of correlated Chi-Square |
| noise | Works for measurement with noise | Both noise free and noise contaminated conditions | Both noise free and noise contaminated conditions |
| accuracy | Least accurate | Accurate for highly-coherent measurements | Accurate for all |
| limitation | More pre-assumptions, hard to satisfy them all | Lower bound penetrates into negative for small estimation | Submerged into noise |

5.0 RECEIVER OPERATING CHARACTERISTICS

Each model may be thus used to determine, with statistical confidence, when damage has occurred. For most of the conditions, the damaged and undamaged distributions are not fully separated, which means at any threshold, there will be both false positives and false negatives. Receiver operating characteristic (ROC) curves visualize the trade-off and help to optimize the best threshold with clear indication of the detection rates. They may also be used to compare the models independently to see which has the best classifier performance.

Consider the model in Figure 7 and the statistical model via Chi-square bivariate approach. Two arbitrary frequency lines are picked at lower and higher frequency regions respectively, as examples to evaluate the probability density and the operating characteristics below. The example frequency points are picked at 0.81 Hz and 3.27 Hz, with a high and low input-output gain, respectively.

Figure 13 lists the probability density evaluations for three noise-contaminated conditions and at two frequency lines. The left column in Figure 13 is evaluated at 0.87 Hz, where the input-output gain factor is large, and the distributions are distinguished very easily, even with 10% noise contamination. In the right hand side column, the curves are barely distinguishable when extraneous noise exists, as all the distributions for different damage levels overlap on top of each other. This is because the transmissibility estimation uncertainty is evaluated at a frequency with low gain factor, and after contamination, the estimation at this frequency is dominated by noise. Therefore, with a change of system parameters, there are no detectable changes in the estimations.

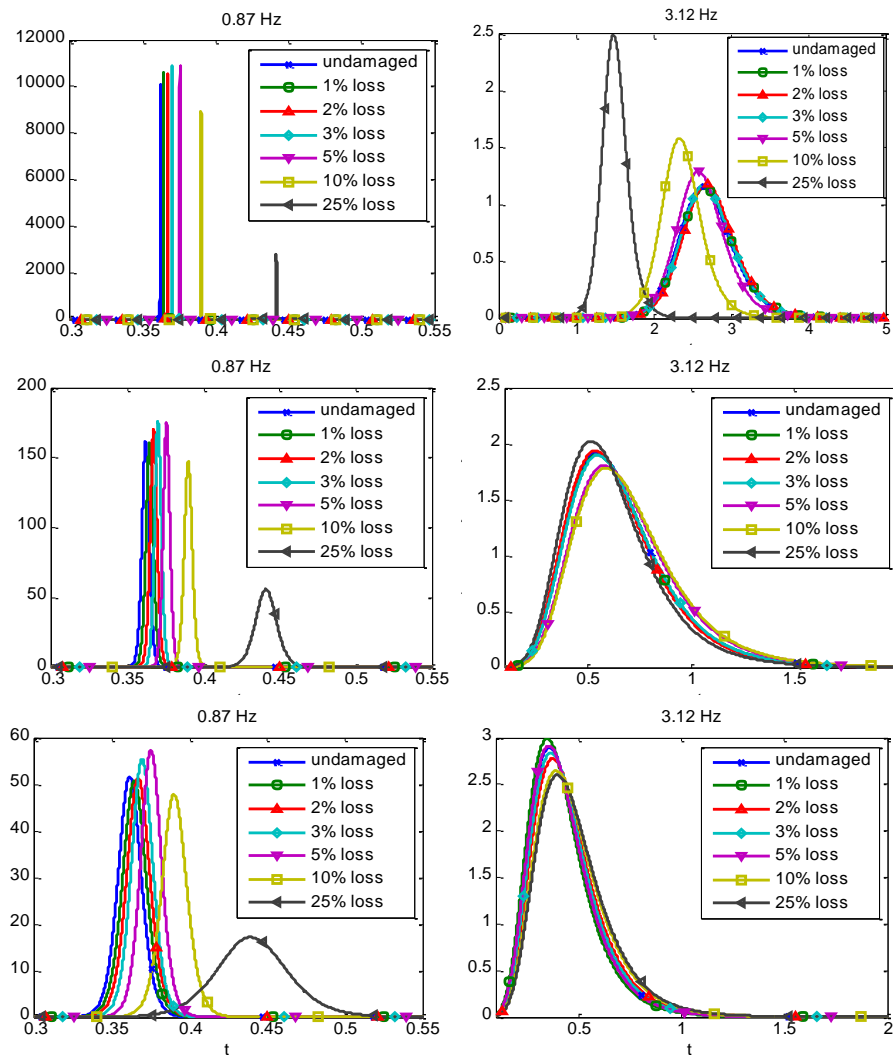


Figure 13: Probability density function of transmissibility estimations for different damage levels, upper left: 0.87Hz, external noise free; mid left: 0.87Hz, 1% NSR; lower left: 0.87Hz, 10% NSR; upper right: 3.12Hz, external noise free; mid right: 3.12Hz, 1% NSR; lower right: 3.12Hz, 10% NSR.

Figure 14 shows the ROC curves for all the conditions in Figure 13, and area-under-curve (AUC) metrics for the entire frequency range are plotted in Figure 15. The larger the AUC (which is computed as the area under the ROC), the better the approach is at globally performing well, i.e., classifying data appropriately. Frequency lines with big gains, especially close to resonances, have both good sensitivity and specificity, i.e. high detection rate with very small false positive rate (type-I error.)

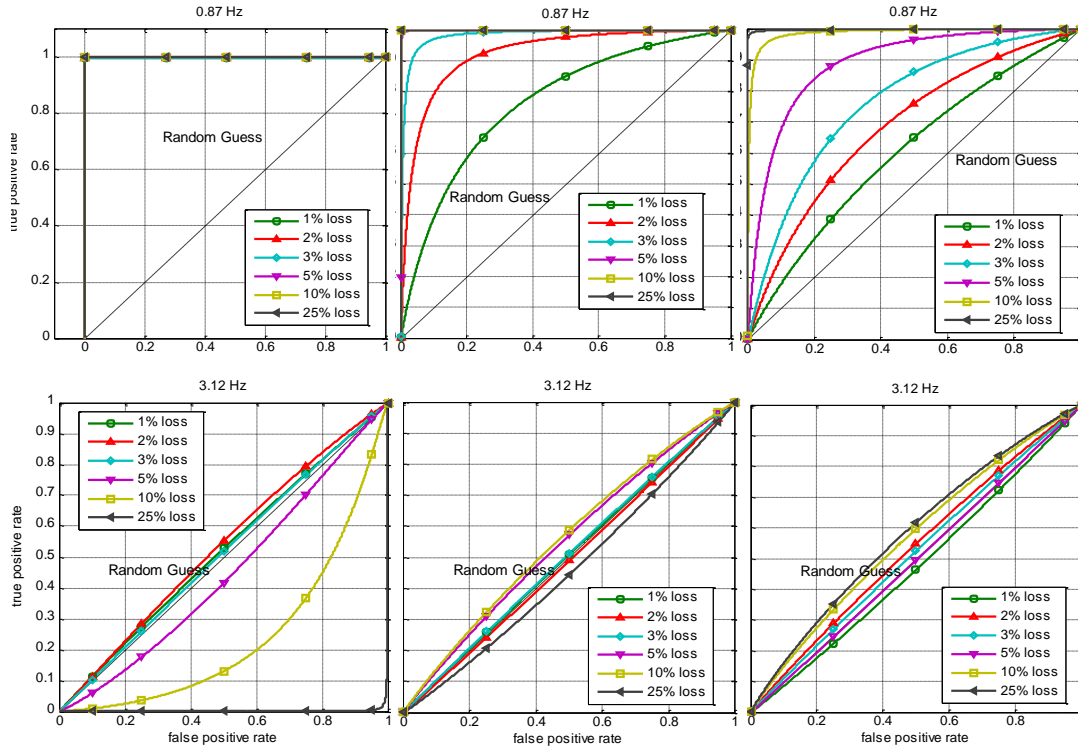


Figure 14: ROC curves for different frequencies and settings with $nd=4$, upper left: 0.87Hz, external noise free; upper mid: 0.87Hz, 1% NSR; upper right: 0.87Hz, 10% NSR; lower left: 3.12Hz, external noise free; lower mid: 3.12Hz, 1% NSR; lower right: 3.12Hz, 10% NSR.

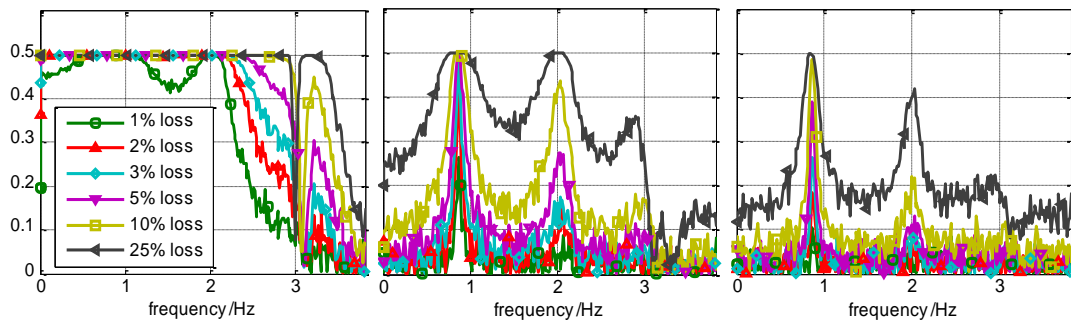


Figure 15: AUC metric evaluation v.s. frequency, left: external noise free; middle: 1% of NSR right: 10% of NSR

Figure 16 compare the AUC metric evaluated at the two example frequency lines, with all the damage conditions included. These results simply indicate the same conclusion that high input-output gain will have better robustness for noise contamination, and will have AUC closer to 0.5, which is the perfect (ideal) value.

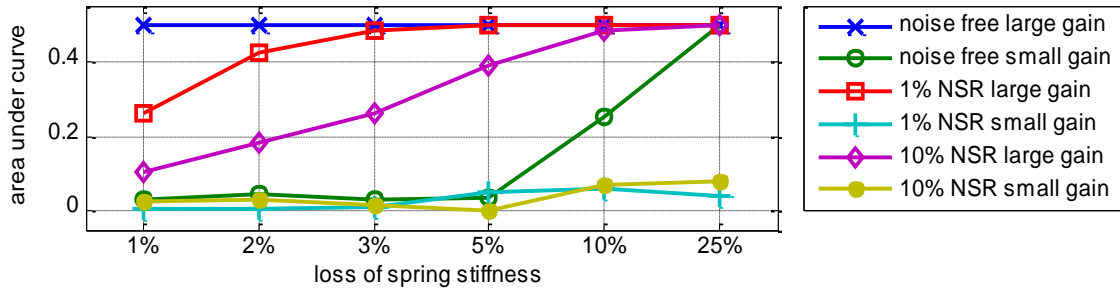


Figure 16: Comparison of AUC for different damage levels and noise-to-signal levels.

6.0 PHASE UNCERTAINTY MODEL

Considering the wide use of phase (not just magnitude, as presented above) in many system identification and modal analysis applications, an uncertainty model of transmissibility phase estimation is also under development. Different from the estimator in Equation (6) in which only magnitude information is contained, another estimator is adopted with respect to cross-power spectra, as shown in Equation (9):

$$T_{ij} = \frac{X^* \cdot V_i}{X^* \cdot V_j} = \frac{G_{xv_i}}{G_{xv_j}}, \quad \text{where } G_{xv} \in \mathbb{E}, \forall i \text{ or } j. \quad (9)$$

The phase estimation is calculated from the ratio between imaginary and real part of the transmissibility estimation:

$$\mathcal{R}[T_{ij}] = \text{atan} 2 \left(\frac{\Im[T_{ij}]}{\Re[T_{ij}]} \right), \quad (10)$$

in which the $\text{atan} 2(\cdot)$ is the four-quadrant arctangent function. The real and imaginary part of the transmissibility, i.e. the denominator and numerator in Equation (10), can be approximated regarded as uncorrelated Gaussian random variables if the test is implemented via a Gaussian process. Therefore, the distribution of phase angle may be obtained from change of variable to arctangent value.

Equation (11) is the final form of the derived probability density function $p(\theta)$:

$$p(\theta) = \sec^2(\theta) \left(\frac{A e^{\left(\frac{C^2}{2B}\right)} \cdot C}{\sqrt{2\pi B^{3/2}}} \operatorname{Erf}\left(\frac{C}{\sqrt{2B}}\right) + \frac{A}{\pi B} \right), \quad (11)$$

where: $A = \frac{1}{2} \left(\frac{\mu_{\text{Re}}^2}{\sigma_{\text{Re}}^2} - \frac{\mu_{\text{Im}}^2}{\sigma_{\text{Im}}^2} \right)$; $B = \frac{1}{\sigma_{\text{Re}}^2} + \frac{\tan^2(\theta)}{\sigma_{\text{Im}}^2}$; $C = \frac{\mu_{\text{Re}}}{\sigma_{\text{Re}}^2} + \frac{\mu_{\text{Im}} \tan(\theta)}{\sigma_{\text{Im}}^2}$. In the probability density function expressed in Equation (11), the parameters are only determined by the mean values and standard deviation of the real and imaginary parts at the corresponding frequency line. One thing that must be clarified is that in order to make the probability density function differentiable, common arctangent function is used, so the range of θ is from $-\pi$ to π . Phase unwrapping beyond this range is accomplished manually.

A real plate structure shaker test was implemented and both uncertainty of transmissibility and transfer function are tested based on Equation (11). The plate is clamped along one edge, and excitation is applied on the blue dot in Figure 17. Four locations of measurements are labeled and marked in brown, and the red dot illustrates the damage position, where an extra spring or mass was added to change the local stiffness/mass. Broadband Gaussian noise is used as the input excitation from shaker.

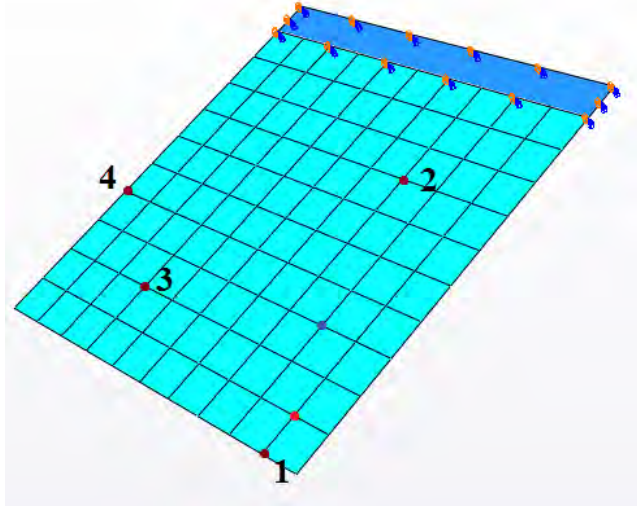


Figure 17: Plate structure illustration.

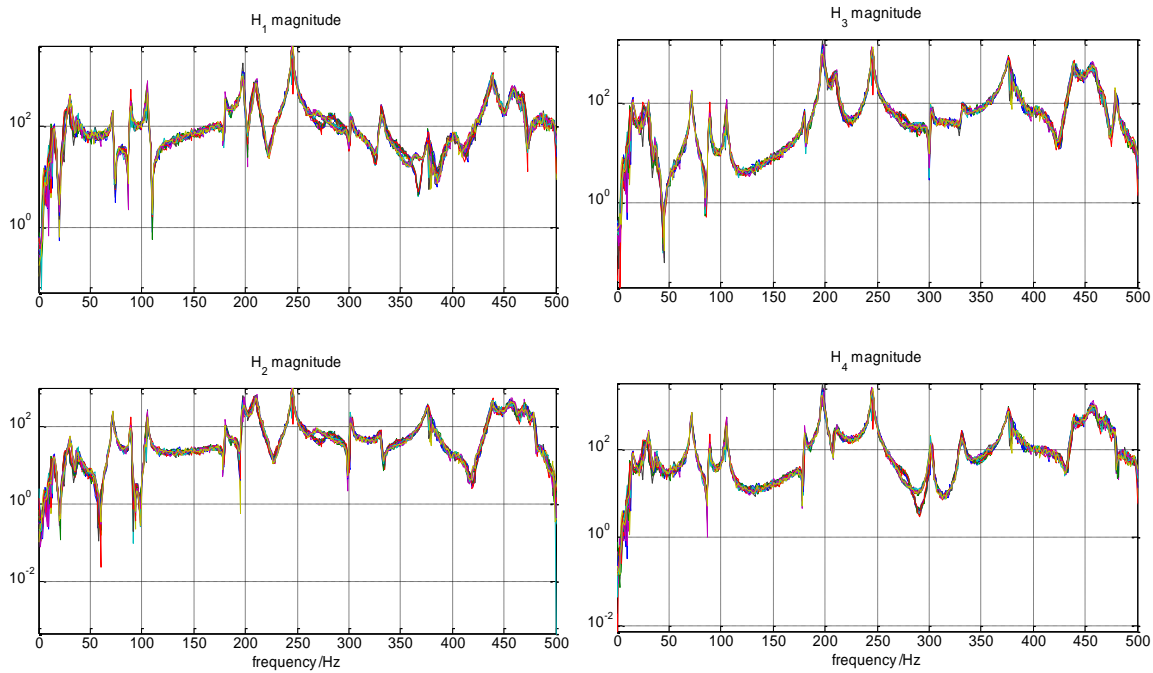


Figure 18: Magnitude of transfer function H , at each measurement point.

Figure 18 and 19 show the magnitude and phase estimations of all the four input-output transfer functions and Figure 20 shows the transmissibility estimations. From both a magnitude and phase point of view, transmissibility is observed to be clearly separated and to be a more sensitive detector of changes caused by system parameter changes due to damage.

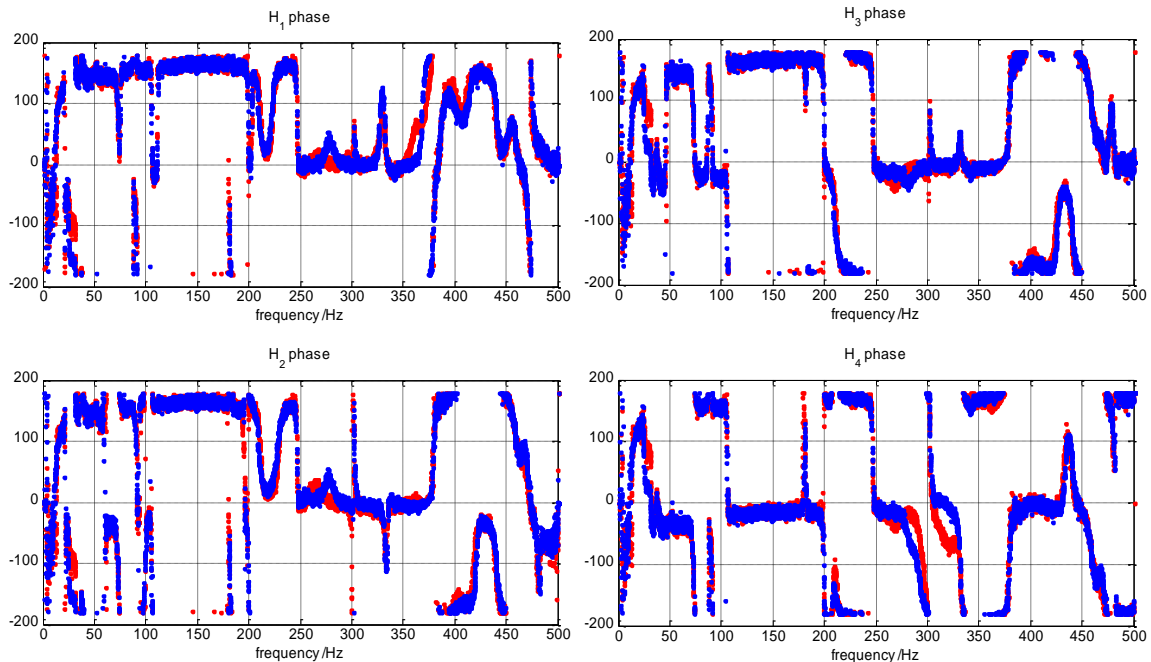


Figure 19: Phase of transfer function H , at each measurement point.

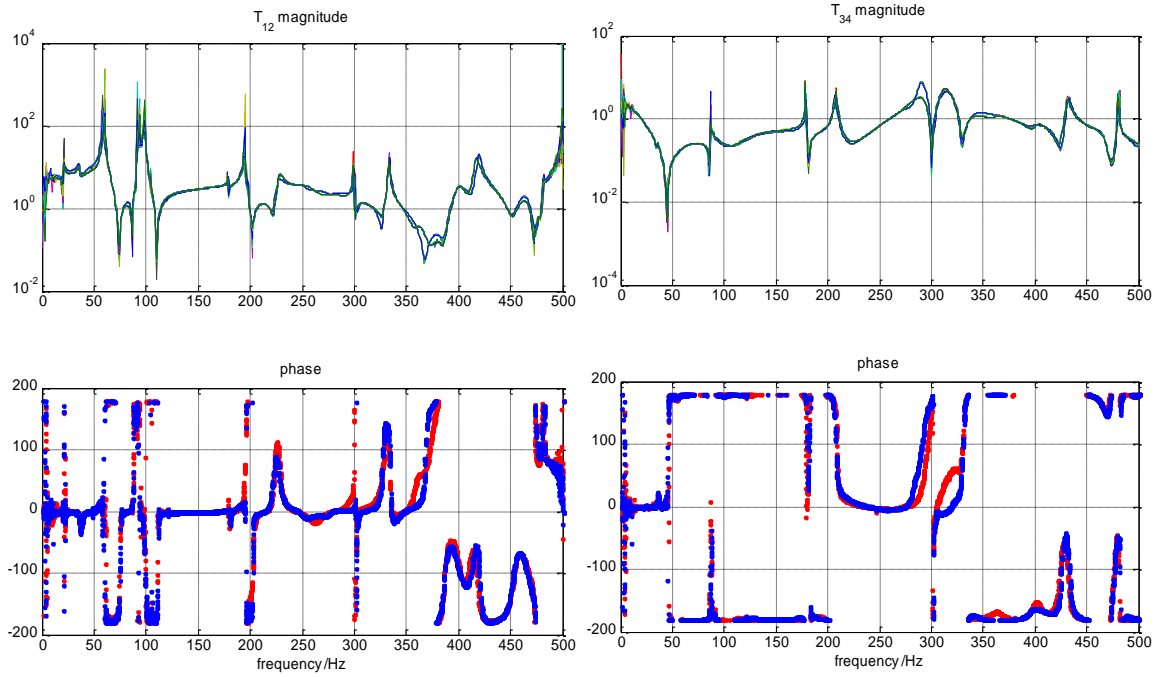


Figure 20: Transmissibility T between 1~2 and 3~4.

The uncertainty model proposed in Equation (11) was validated by the real measurement data obtained from plate structure characterized in Figure 17, and the phase uncertainty of both transfer function and transmissibility were tested.

Figure 21 illustrates the histogram of phase estimation at arbitrary frequency lines, for transfer function H and transmissibility T , where the red curve is the predicted distribution calculated from Equation (11). The histogram coincides perfectly with the predicted curves.

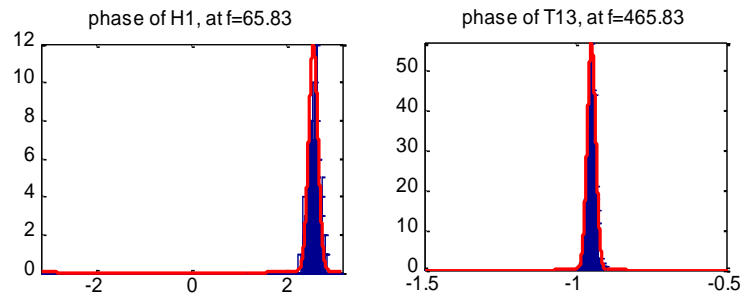


Figure 21: Histogram of phase estimation for H and T at arbitrary frequency lines.

Similar to magnitude uncertainty quantification, using the statistical model given by Equation (11), the 90% confidence boundaries of phase estimations are plotted in Figure 22, with undamaged estimation in blue and damaged estimation in red, and the corresponding outlier percentage at each frequency line is also plotted to the right. The outlier percentages for

undamaged case are plotted in blue dots, and the damaged case is in green. Red line represents the pre-set confidence threshold, which is 10% in Figure 22.

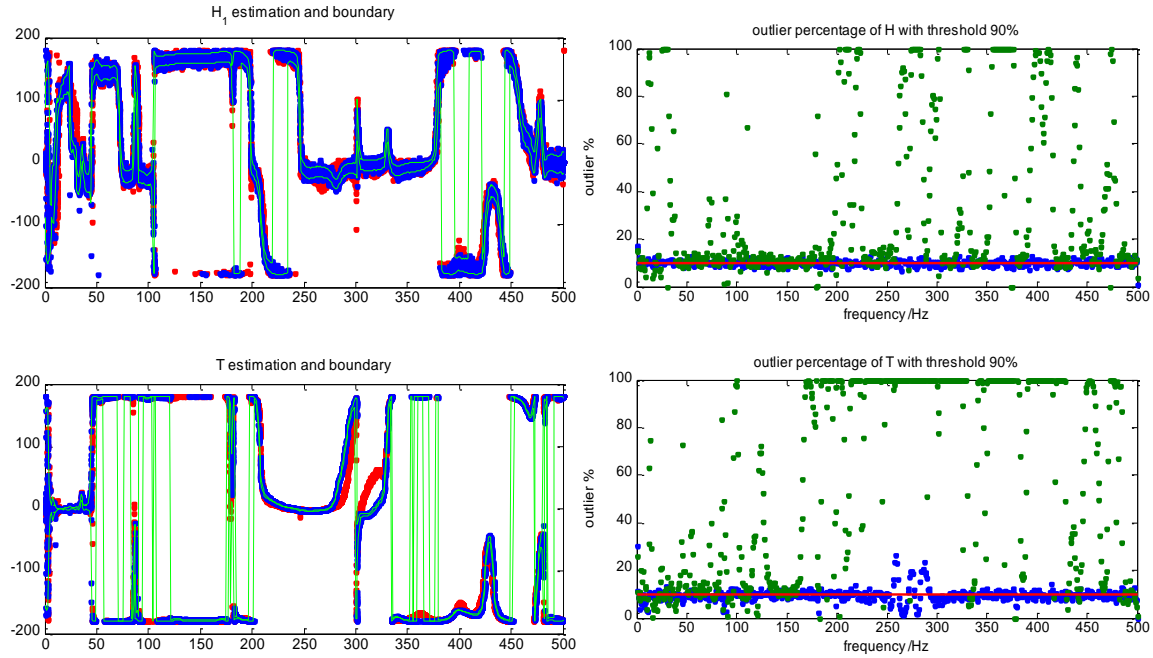


Figure 22: Magnitude of transfer function H , at each measurement point.

Figure 22 shows that the phase estimation for transfer function has larger variation than transmissibility phase, and the uncertainty bounds capture this issue. For the outlier percentages on the right-hand side subplots, the undamaged (blue) results show very good consistency with the anticipated value, except for transmissibility phase estimations in a small area (250~300Hz) where the Gaussian assumption does not hold very well. Green dots in Figure 22 show the outlier percentages for the damaged condition, using the same bounds as undamaged case. A lot more outliers are observed, especially for transmissibility observations. This illustrates that transmissibility has less phase estimate uncertainty and is more sensitive to structural damage.

To be more quantitative in comparing the outlier percentage, two metrics as expressed in Equation (12) and (13) are also defined, which are respectively the average outlier percentage over all the frequency lines and the mean square error of the outlier percentage offsetting from the pre-set threshold q , which is 10% here:

$$\overline{pct} = \frac{1}{n} \sum_{k=1}^n (pct_{(k)} - q), \quad (12)$$

$$MSE = \sum_{k=1}^n (pct_{(k)} - q)^2, \quad (13)$$

where n is the total number of frequency bins and $pct_{(k)}$ is the outlier percentage at k^{th} frequency line as shown in Figure 22

Figure 23 and 24 compare the metrics defined in Equation 12 and 13, both damaged and undamaged conditions, and a very clear separation between the two groups of data is observed. This study was still ongoing at the termination of funding for this project.

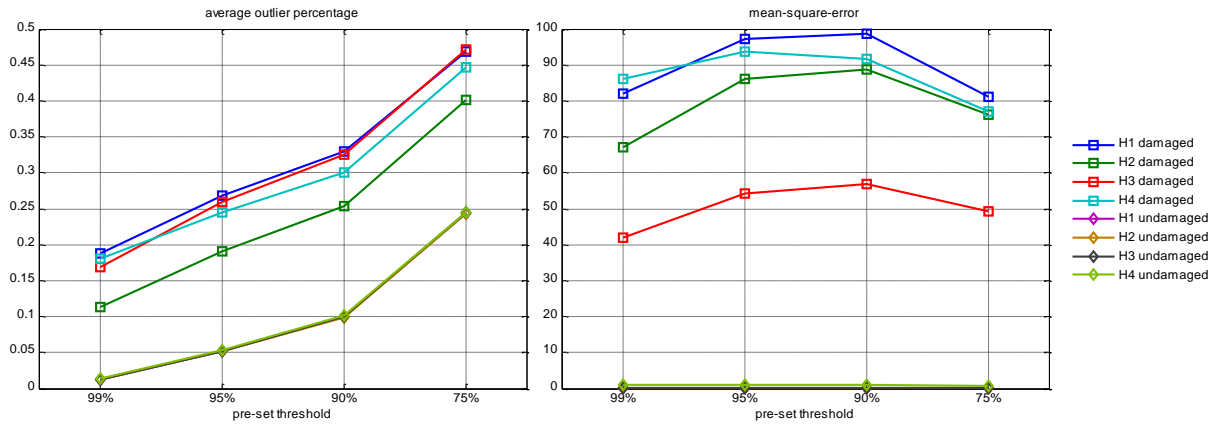


Figure 23: Metrics of transfer function phase estimation.

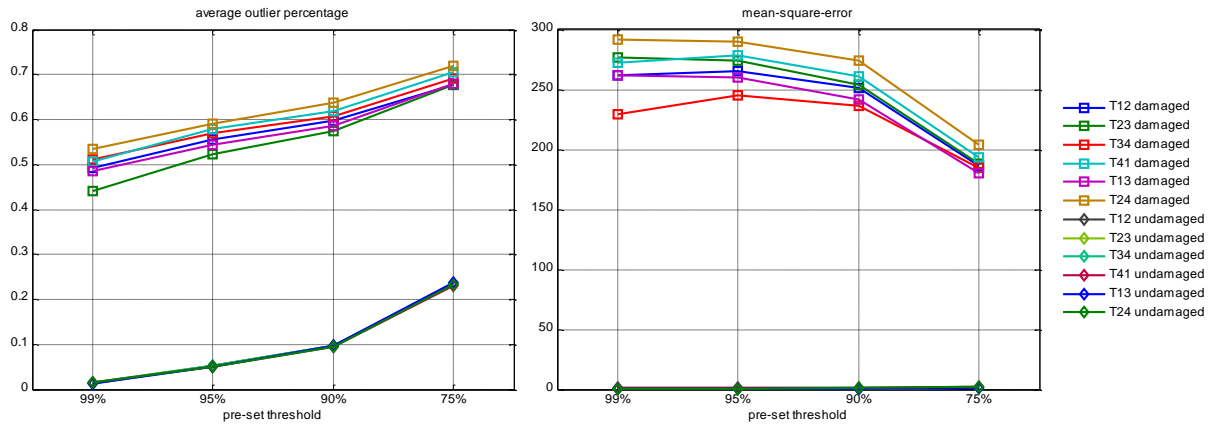


Figure 24: Metrics of transmissibility phase estimation.

7.0 CONCLUSIONS

The model via perturbation approach simply supplies the variance and bias error for one of the transmissibility estimators, which requires the least information about input and output. Gaussian bivariate approach gives a more accurate quantification through cross power density estimations, except in very small frequency range, where the magnitude is really low and does not deliver lots of useful information. Chi-square bivariate approach delivers the most accurate statistical model and does not require any information from the input, but when extraneous noise level is high, the estimator itself is dominated by the noise floor, and does not contain useful transmissibility information. Furthermore, although this approach had overall the best features, it only works for transmissibility magnitude estimations. All comparisons were validated on a three-degree-of-freedom system model.

Based upon the statistical models established, a receiver operating characteristic (ROC) analysis was applied to evaluate performance, and the conclusion was reached that at frequency lines with good input-output gain, the detection is globally stable even when there is noise contamination.

Phase estimation statistical modeling work commenced for both frequency response function and transmissibility. Similar validation has been done with data from a cantilevered plate structure. Test results show clearly the sensitivity of transmissibility phase in capturing structural parameter changes, although this study was still ongoing at the time of funding loss.

8.0 RECOMMENDATIONS AND FUTURE WORK

The recommendations from this work are the following:

1. Use the Chi-square bivariate model when transmissibility magnitude is being estimated.
2. Use the Gaussian ratio model when transmissibility phase is being estimated.

Future work is considered to be propagation of the uncertainty from the current spectral estimations, transfer function and transmissibility, to the structural health monitoring features, such as the root mean square error and dot product difference proposed in the first part of this project. Analytical models might not be available because of the mathematical complexity, and focus will be made upon Monte Carlo modeling, mixture modeling, and meta-analysis.

Several publications resulted from this project:

Z. Mao and M. D. Todd, "A Model for Quantifying Uncertainty in the Estimation of Noise-Contaminated Measurements of Transmissibility," *Mechanical Systems and Signal Processing*, in press, 2011.

Z. Mao and M. D. Todd, "A Statistical Confidence Model for Noise-Contaminated Structural Transmissibility Measurements Used in Damage Detection," *Proc. SPIE Smart Structures/NDE 7650*, San Diego, California, March 8-11, 2010.

Z. Mao and M. D. Todd, "A Model of Uncertainty Quantification in the Estimation of Noise-Contaminated Transmissibility Measurements for System Identification", *Proceedings of IMAC XXIV: A Conference on Structural Dynamics*, Jacksonville, Florida, January 31-February 3, 2011. **(DEMICHELE AWARD)**

Z. Mao and M. D. Todd, "Uncertainty Quantification in Transmissibility-Derived Features Used for Fault Detection," *8th International Workshop on Structural Health Monitoring*, Stanford, California, September 13-15, 2011.

REFERENCES

- [1] L. Ljung, "Aspects on the system identification problem," *Signal Processing*, 4, 445-456, 1982.
- [2] R. Brincker, L. Zhang, P. Andersen, "Modal identification of output-only systems using frequency domain decomposition," *Smart Materials and Structures*, 10, 441-445, 2001.
- [3] S.W. Doebling, C.R. Farrar, M.B. Prime, "A summary review of vibration-based damage identification methods," *The Shock and Vibration Digest*, 30(2), 91-105, 2002.
- [4] C. Devriendt, G. Steenackers, G. De Sitter, P. Guillaume, "From operating deflection shapes towards mode shapes using transmissibility measurements," *Mechanical Systems and Signal Processing*, 24, 665-677, 2010.
- [5] T.J. Johnson, D.E. Adams, "Transmissibility as a differential indicator of structural damage," *Transactions of the ASME: Journal of Vibration and Acoustics*, 124, 634-641, 2002.
- [6] C. Devriendt, P. Guillaume, "Identification of modal parameters from transmissibility measurements," *Journal of Sound and Vibration*, 314, 343-356, 2008.
- [7] A.M.R. Ribeiro, J.M.M. Silva, N.M.M. Maia, "On the generalisation of the transmissibility concept," *Mechanical systems and Signal Processing*, 14, 29-35, 2000.
- [8] J.E. Mottershead, "On the zeros of structural frequency response functions and their sensitivities," *Mechanical Systems and Signal Processing*, 12, 591-597, 1998.
- [9] J. He, Y.-Q. Li, "Relocation of anti-resonance of a vibratory system by local structural changes," *Modal Analysis: the International Journal of Analytical and Experimental Modal Analysis*, 10, 224-235, 1995.
- [10] C. Devriendt, P. Guillaume, "The use of transmissibility measurements in output-only modal analysis," *Mechanical Systems and Signal Processing*, 21, 2689-2696, 2007.
- [11] T.J. Johnson, "Analysis of Dynamic Transmissibility as a Feature for Structural Damage Detection," M.S. Thesis, Purdue University, 2001.
- [12] R.L. Brown, D.E. Adams, "Equilibrium point damage prognosis models for structural health monitoring," *Journal of Sound and Vibration*, 262, 591-611, 2003.
- [13] K. Worden, "Structural fault detection using a novelty measure," *Journal of Sound and Vibration*, 201, 85-101, 1997.
- [14] D. Afolabi, "An anti-resonance technique for detecting structural damage," *Proceedings of the 5th International Modal Analysis Conference*, 491-495, 1987.

- [15] K. Worden, G. Manson, N.R.J. Fieller, Worden K, Manson G, Fieller NRJ, "Damage detection using outlier analysis," *Journal of Sound and Vibration*, 229(3), 647-667, 2000.
- [16] K. Worden, G. Manson, D.J. Allman, "Experimental validation of a structural health monitoring methodology, Part I: novelty detection on a laboratory structure," *Journal of Sound and Vibration*, 259, 323-343, 2003.
- [17] G. Manson, K. Worden, D.J. Allman, "Experimental validation of a structural health monitoring methodology, Part II: novelty detection on a GNAT aircraft," *Journal of Sound and Vibration*, 259, 345-363, 2003.
- [18] G. Manson, K. Worden, D.J. Allman, "Experimental validation of a structural health monitoring methodology. Part III: damage location on an aircraft wing," *Journal of Sound and Vibration* 259, 365-385, 2003.
- [19] H. R. Kess, D.E. Adams, "Investigation of operational and environmental variability effects on damage detection algorithms in a woven composite plate," *Mechanical Systems and Signal Processing*, 21, 2394-2405, 2007.
- [20] J. S. Bendat, A.G. Piersol, *Random Data: Analysis and Measurement Procedures*, 2nd Edition, John Wiley & Sons, New York, 1986.
- [21] J. S. Bendat, A.G. Piersol, *Engineering Applications of Correlation and Spectral Analysis*, 2nd Edition, John Wiley & Sons, New York, 1993.
- [22] J. S. Bendat, "Statistical errors in measurement of coherence function and input/output quantities," *Journal of Sound and Vibration*, 59, 405-421, 1978.
- [23] T. Schultz, M. Sheplak, L.N. Cattafesta III, "Application of multivariate uncertainty analysis to frequency response function estimates," *Journal of Sound and Vibration*, 305, 116-133, 2007.
- [24] N. R. Goodman, "Statistical analysis based on a certain multivariate complex Gaussian distribution (an introduction)," *Annals of Mathematical Statistics*, 34, 152-177, 1963.
- [25] N. R. Goodman, "Measurement of matrix frequency response functions and multiple coherence functions," *Measurement Analysis Corp., Tech. Rept. AFFDL-TR-65-56*, June 1965.

DISTRIBUTION LIST

| | |
|--|-------|
| DTIC/OCF 8725 John J. Kingman Rd, Suite 0944 Ft Belvoir, VA 22060-6218 | 1 cy |
| AFRL/RVIL Kirtland AFB, NM 87117-5776 | 2 cys |
| Official Record Copy AFRL/RVSV/Whitney Reynolds | 1 cy |